Alternative back contacts in kesterite Cu 2 ZnSn(S 1-x Se x) 4 thin film solar cells

G. Altamura, L. Grenet, Charlotte Roger, F. Roux, V. Reita, R. Fillon, H. Fournier, S. Perraud, H. Mariette

Journal of Renewable and Sustainable Energy

Alternative back contacts in kesterite $Cu_2ZnSn(S_{1-x}Se_x)_4$ thin film solar cells

Cite as: J. Renewable Sustainable Energy **6**, 011401 (2014); https://doi.org/10.1063/1.4831781
Submitted: 05 August 2013 . Accepted: 01 November 2013 . Published Online: 11 February 2014

G. Altamura, L. Grenet, C. Roger, F. Roux, V. Reita, R. Fillon, H. Fournier, S. Perraud, H. Mariette, et al.

Alternative back contacts in kesterite $Cu_2ZnSn(S_{1-x}Se_x)_4$ thin film solar cells

G. Altamura,[1,2,a)] L. Grenet,[1] C. Roger,[1] F. Roux,[1] V. Reita,[3] R. Fillon,[1] H. Fournier,[1] S. Perraud,[1] and H. Mariette[1,2,3]
[1]*CEA, 17 rue des Martyrs, 38054 Grenoble Cedex 9, France*
[2]*Université Joseph Fourier, 38041 Grenoble Cedex 9, France*
[3]*Institut Néel, CNRS, 25 rue des Martyrs, 38054 Grenoble Cedex 9, France*

(Received 5 August 2013; accepted 1 November 2013; published online 11 February 2014)

Molybdenum (Mo) is the most used back contact in $Cu_2ZnSn(S_{1-x}Se_x)_4$ based solar cells. However, it has been suggested recently that Mo is not stable at the interface with $Cu_2ZnSn(S_{1-x}Se_x)_4$. In addition, to the best of our knowledge, no experimental study has been carried out so far to test whether solar cells built on another back contact could exhibit better photovoltaic properties. For this purpose, various metals (Au, W, Pd, Pt, and Ni) are deposited on top of Mo, and it is demonstrated that it is possible to synthesize device-quality $Cu_2ZnSn(S_{1-x}Se_x)_4$ thin films on W, Au, and Pt back contacts. It is shown that that W and Au back contacts allow enhancing the photogenerated current, but that Mo remains the best back contact in terms of power conversion efficiency. © *2014 AIP Publishing LLC*.
[http://dx.doi.org/10.1063/1.4831781]

I. INTRODUCTION

$Cu_2ZnSn(S_{1-x}Se_x)_4$ (CZTSSe) alloys are promising candidates for low-cost and high-efficiency thin film solar cells since most elements are abundant in the earth crust and encouraging photovoltaic (PV) device performances have been obtained recently. Some of the CZTSSe characteristics are a direct bandgap[1] between around 1 eV ($Cu_2ZnSnSe_4$) and around 1.5 eV (Cu_2ZnSnS_4), and an absorption coefficient larger than $10^4\,cm^{-1}$.[2–4] With these properties, 11.1% efficient devices have already been demonstrated.[2]

In most of the publications dealing with CZTSSe thin films for PV applications, the structure of the solar cell is directly copied from those used in $Cu(In,Ga)Se_2$ (CIGS) technology. Especially, molybdenum (Mo) is used as back contact (BC), but this choice has not been optimized for CZTSSe.

The properties of the BC have a strong impact on the solar cell performances. Patel and Ray[5] simulated numerically the current-voltage (J-V) characteristics of a Al:ZnO/i-ZnO/CdS/CZTSSe/BC solar cell trying to find the optimum BC material and CZTSSe layer thickness which gives the best cell performances. SCAPS software simulations[6] showed that solar cell performances are improved by increasing the BC work function. According to these simulations, Mo is not the best BC in terms of power conversion efficiency. On the other hand, Scragg *et al.*[7] suggested reexamining the choice of molybdenum due to a phase-segregation at CZTSSe|Mo interface during annealing.

Those works have motivated the present article in which we have studied experimentally the effects of different back contacts on the performances of CZTSSe solar cells. In this study several metals (Au, W, Pd, Pt, and Ni) have been deposited on top of a Mo thin film in order to study: (i) the possibility of synthesizing CZTSSe on different BC, (ii) the interaction of the BC with the chalcogens during the selenization process, and (iii) the influence of the BC on Al:ZnO/i-ZnO/CdS/CZTSSe/BC/Mo solar cell performances.

[a)]Author to whom correspondence should be addressed. Electronic mail: giovanni.altamura@cea.fr. Tel.: +33(0)4-38-78-14-68.

II. EXPERIMENTAL DETAILS

Substrates used in this study are those commonly employed in CZTSSe based solar cell technology: Mo-coated soda-lime glass substrates deoxidized for 10 s in a 10% NH_3. Two different techniques are used to deposit 100 nm-thick BC: W and Au are deposited via DC-sputtering in a Plassys MP400 system at 1×10^{-3} millibar of Ar at room temperature, while Pd, Pt, and Ni are deposited by high vacuum electron-beam evaporation in a Plassys MEB550S deposition chamber at 5×10^{-7} millibars. In both cases deposition rates are controlled by a quartz balance. It should be noted that in this study, the 100-nm-thick BC (Au, W, Pt, Pd, and Ni) is deposited on top of a 400-nm-thick Mo layer. There are three reasons to keep an underlying Mo layer: (i) some metals like for example Pd and Pt do not have a good adhesion on soda-lime glass, (ii) we assume that Mo may play a role of barrier for contaminant from glass (in order to be more confident that the CZTSSe performances do not suffer from excess of contamination, we prefer to have the same potential barrier), and (iii) in the context of low-cost solar cells like CZTSSe-based ones, the interest of an alternative back contact may only exist if the new back contact is not expensive; due to the cost of the metals used in this work (except W), it could be of interest to add a (very) thin interfacial layer between Mo and CZTSSe but not to replace the 400-nm-thick Mo layer.

CZTSSe is synthesized on the different BC by selenization of vacuum deposited precursors. A ZnS layer is deposited via RF-sputtering,[8] while metallic layers of Cu and Sn are grown by high vacuum electron-beam evaporation.[8,16] In both cases deposition rates are controlled by a quartz balance.

The precursor selenization to synthesize CZTSSe layers occurs in a tubular furnace under Ar atmosphere at a temperature of 570 °C. The typical annealing time at 570 °C of 30 min results in a total annealing process of about 1 h. Selenium is provided in the form of pellets put beside the precursors in order to assure the selenization process.

The precursor deposition and selenization method to synthesize CZTSSe are described in Ref. 8, and they allow obtaining a CZTSSe alloy with about 90% Se and 10% S as measured by energy-dispersive X-ray spectroscopy (EDS) (results not shown here).

Solar cells are completed by adding a 70-nm-thick CdS layer grown by chemical bath deposition to form the hetero-junction, a 50-nm-thick i-ZnO layer and a 450-nm-thick Al:ZnO layer grown by sputtering from a pure ZnO target and from a 2 wt. % Al_2O_3-ZnO target, respectively.

A Karl Zeiss Leo 1530 scanning electron microscope (SEM) is used to examine the morphology of CZTSSe layers as well as estimate their thicknesses. Crystallographic properties of the material are characterized by X-ray diffraction (XRD) in a D8 Advance Bruker AXS and by confocal Raman spectroscopy in a Horiba Jobin Yvon LabRAM-HR 800 spectrometer in backscattering configuration with a 10 mW 532 nm green laser excitation. A Horiba glow discharge spectroscopy (GDS) tool is used to evaluate the depth profile of each element in the material. The photovoltaic performances are evaluated under standard AM 1.5 illumination with a Spectra-Nova's CT Series Solar Cell Tester at 25 °C. External quantum efficiency (EQE) measurements are carried out in a Lot Oriel Spequest with a monochromator under chopped illumination and a lock-in technique.

III. RESULTS AND DISCUSSIONS

Fig. 1 shows GDS spectra of CZTSSe synthesized on different BCs. Palladium and nickel (CZTSSe|Pd and CZTSSe|Ni in Figs. 1(d) and 1(e), respectively) diffuse into the CZTSSe reaching the surface of the sample. The diffusion of Ni through the absorber layer has been already noticed also for CIGS solar cells.[9] On the contrary, Au, W, and Pt remain in contact with Mo. In the case of Au (CZTSSe|Au in Fig. 1(a)), the Mo signal is not equal to zero far from the BC: This is an artifact of the GDS experiment, due to the presence of voids in the CZTSSe layer at the measured point. In the case of W (CZTSSe|W in Fig. 1(b)) we can see an important superposition of W with S and Se profiles. Finally for Pt (CZTSSe|Pt), there is a clear superposition of the Pt and Se profiles (Fig. 1(c)).

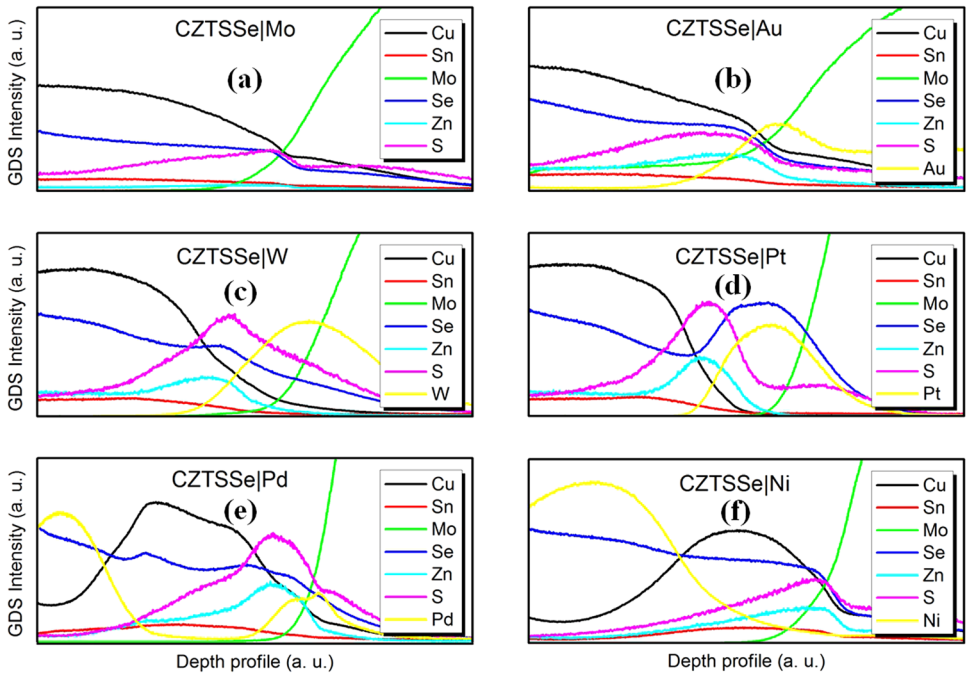

FIG. 1. GDS spectra of CZTSSe synthesized on Mo (CZTSSe|Mo) (a), Au (CZTSSe|Au) (b), W (CZTSSe|W) (c), Pt (CZTSSe|Pt) (d), Pd (CZTSSe|Pd) (e), and Ni (CZTSSe|Ni) (f).

Hereinafter only characterization made on CZTSSe on Au, W, and Pt are presented since it has been demonstrated that CZTSSe grown on Pd and Ni is not of interest due to their diffusion towards the surface.

Crystallographic properties of the material are characterized by XRD. Fig. 2 shows the diffraction spectra of CZTSSe grown on Au, W, and Pt. The CZTSSe patterns[10] are recognizable by the main reflections at 22.0°, 27.2°, 33.8°, 45.1°, and 53.5° which are visible in all the spectra; the reflection of Mo is at 40.2° and 87.4°.[10] In the case of CZTSSe on Au (CZTSSe|Au),

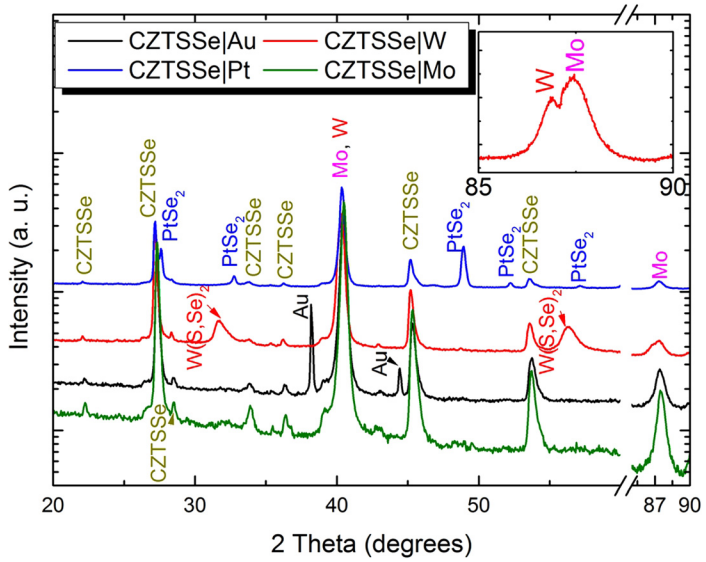

FIG. 2. XRD patterns of CZTSSe synthesized on Mo (CZTSSe|Mo), Au (CZTSSe|Au), W (CZTSSe|W), and Pt (CZTSSe|Pt). Patterns are shifted vertically and the x-axis is cut between 60° and 85° for clarity. The inset shows a zoom on CZTSSe|W in the range of 85°–90°.

the Au peaks at 38.2° and 44.6° are visible. It should be noted that no gold-chalcogens phases are detected pointing the fact that Au BC has not reacted with neither S nor Se during the selenization process. In the case of CZTSSe on W (CZTSSe|W), the W reflection at 39.9° (Ref. 11) overlaps with the Mo one since they have almost the same lattice constants but at higher diffraction angles it is possible to discern W (86.9°) from Mo (87.4°) (inset in Fig. 2) which proves that metallic W is still present. Moreover, $W(S,Se)_2$ peaks are present, respectively, at 32.0° and 56.5° (Ref. 12) indicating the W has reacted with sulfur and selenium, which is consistent with the GDS spectrum (see the overlap of W, S, and Se profiles in Fig. 1(b). Finally for CZTSSe on Pt, the reflections at 32.8° and 48.6° are signatures of the $PtSe_2$ phase;[10] again, this is consistent with the GDS spectrum (see the overlap of Pt and Se profiles in Fig. 1(c)). No peaks of metallic Pt are visible.

To sum up, XRD analysis discloses that: (i) Au does not react with chalcogens, (ii) W reacts but not completely, and (iii) Pt completely reacts.

Figure 3 shows Raman analysis made on CZTSSe grown on Au (Fig. 3(a)), W (Fig. 3(b)), and Pt (Fig. 3(c)). Raman spectra of CZTSSe|Au and CZTSSe|W show the same profiles indicating both the peak of $Cu_2ZnSnSe_4$ at 197 cm^{-1} which could be assigned to the A1 mode of kesterite,[13] and the peak of Cu_2ZnSnS_4 (CZTS) at 329 cm^{-1}.[14] This is in good agreement with the bimodal behavior of the CZTSSe alloy already observed by Grossberg *et al.*[15] Other signatures of CZTSe are present in the range of 174–176 cm^{-1} and 234–236 cm^{-1}.[14]

In the case of CZTSSe|Pt, the spectrum is more complicated with broader CZTSSe related peaks and additional ones.

As no Raman spectrum of $PtSe_2$ is found in the literature, a 100-nm-thick layer of Pt has been selenized and then characterized by XRD confirming the formation of a single phase of $PtSe_2$. Then Raman spectrum of this pure $PtSe_2$ sample is acquired and used to further characterize CZTSSe|Pt (inset in Fig. 3). It is noticeable in the Raman spectra that the peaks at 205 cm^{-1} and 177 cm^{-1} are signatures of $PtSe_2$. The kesterite peaks of $Cu_2ZnSnSe_4$ and Cu_2ZnSnS_4 are also visible (at 195 cm^{-1} and 328 cm^{-1}, respectively) but with a widening of

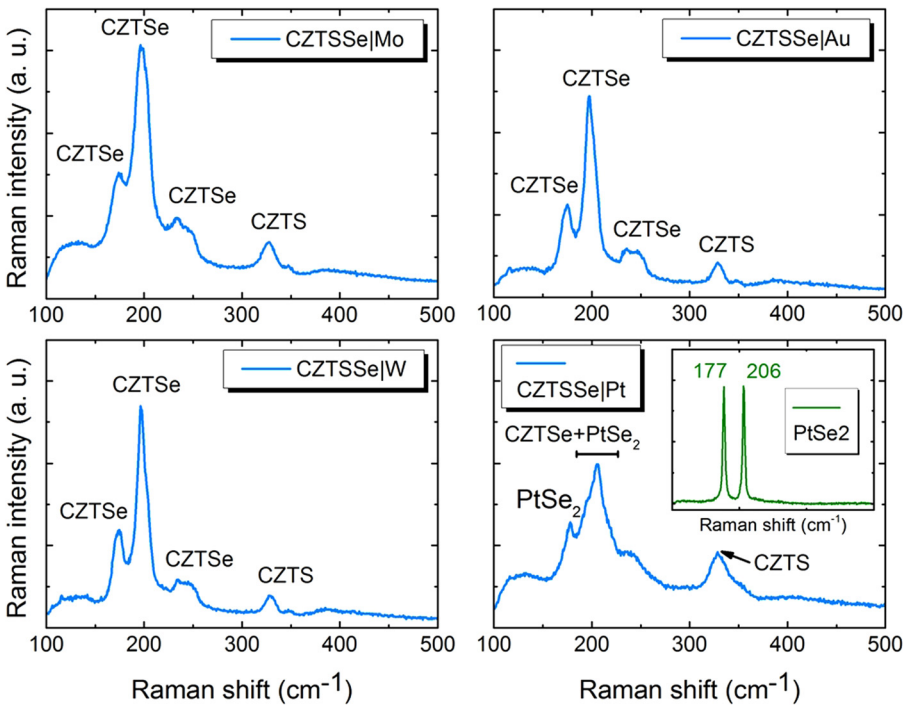

FIG. 3. Raman spectra of CZTSSe synthesized on Mo (CZTSSe|Mo) (top-left), Au (CZTSSe|Au) (top-right), W (CZTSSe|W) (bottom-left), and Pt (CZTSSe|Pt) (bottom-right). The inset in the bottom-right of Fig. 3 shows the Raman spectrum of $PtSe_2$.

their own signal, which is an indication of a low crystallographic quality. $PtSe_2$ is visible although the 1 μm CZTSSe layer should absorb the laser signal since many voids are present at the surface as observed in SEM (not shown here).

SEM cross-section images of CZTSSe|Au, CZTSSe|W, and CZTSSe|Pt samples are shown in Fig. 4. For the CZTSSe|Au sample (Fig. 4(a)), the 1.1 μm thick CZTSSe layer is apparently in direct contact with the Mo and the 100 nm layer of gold is not visible after selenization process. But it is also noticed on the SEM images that, in some zones where there is a gap between the CZTSSe layer and the Mo layer, particles with a diameter around 270 nm appear (inset in Fig. 4(a)). These particles are identified as gold by cross-sectional EDS (not shown here). During the selenization process, the 100-nm-thick gold layer is dewetted to form gold particles on the bottom of the absorber with an estimated mean distance of 300 nm among them. This dewetting occurs during the annealing process since it was a uniform layer after precursor deposition as confirmed by SEM images. This Au dewetting process allows Mo to be exposed to the incoming Se during annealing. CZTSSe|W SEM image (Fig. 4(b)) shows a 1.1-μm-thick CZTSSe layer and a 350-nm-thick layer detected on the top of Mo: according to the results obtained by GDS and XRD, part of it could be assigned to a $W/W(S,Se)_2$ phase. In the case of the CZTSSe|Pt sample (Fig. 4(c)), according to the previous characterizations, the layer detected on the top of Mo is assigned to $PtSe_2$; as for CZTSSe|W, big CZTSSe grains are visible. Noteworthy are, in the three cases (Fig. 4), the small grains at the interface between CZTSSe and BC. These small grains have been attributed to a Zn-rich phase.[16]

After these characterizations CZTSSe|Au, CZTSSe|W, and CZTSSe|Pt are employed in full PV devices, at least eight 0.25 cm^2 solar cells have been fabricated and electrically characterized for each CZTSSe|BC combination and compared with CZTSSe solar cells built on a standard Mo BC. In Figs. 5(a) and 5(b), light J-V characteristics are depicted for all the cells. First, it is noticeable that solar cells built on Pt exhibit very low performances and will be excluded from the following discussion. These low performances could be the effect of a low crystallographic quality CZTSSe as demonstrated by Raman spectroscopy and because of the voids in the absorber as mentioned before.

The median power conversion efficiency (PCE) in the case of Mo is higher compared to the other BC (Au and W) and the dispersion of results is smaller. The variation of PCE between cells with different BC is clearly dominated by the variation of the fill factor (FF) (Fig. 5(a)). To check the possible implications of parasitic resistances in the FF, dark J-V measurement has been carried out. Fig. 5(c) discloses series resistance (R_s), shunt resistance (R_{sh}), and dark saturation current (J_0) extracted from dark J-V characteristics of CZTSSe|Mo-, CZTSSe|W-, and CZTSSe|Au-based solar cells: in the case of W, the median R_s is 4 times higher than in the case of Mo probably due to the thick $W/W(S,Se)_2$ layer (see Fig. 4(b)). In the case of Au, the very low R_{sh} (ascribed to the high density of voids in the stack, see Fig. 4(a)) may be responsible for the low FF.

The BC does not have a clear influence on the J_0. Actually the J_0 median value seems to be slightly higher in the case of Mo, but the extraction of this parameter is subject of an important uncertainty because of the parasitic resistances and we assume that the small variation is

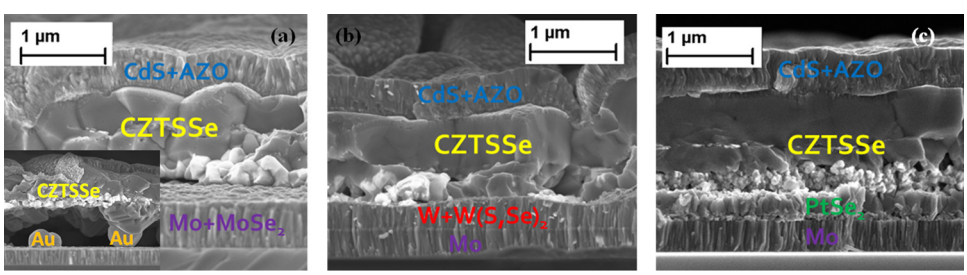

FIG. 4. SEM images of Al:ZnO/i-ZnO/CdS/CZTSSe/BC/Mo solar cells synthesized on Au (CZTSSe|Au) (a), W (CZTSSe|W) (b), and Pt (CZTSSe|Pt) (c). The inset in Fig. 4(a) shows the SEM image of gold particles after selenization process.

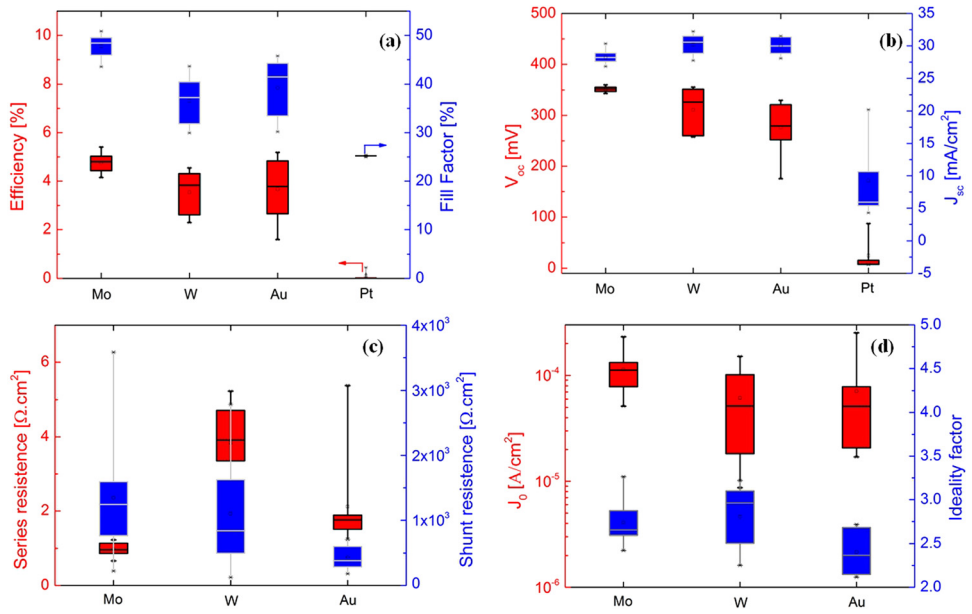

FIG. 5. Current-voltage measurements under illumination (simulated AM1.5 spectrum, 100 mW/cm^2) of Al:ZnO/i-ZnO/CdS/CZTSSe/BC/Mo solar cells: efficiency and fill factor (a), open-circuit voltage (V_{oc}) and short-circuit current (J_{sc}) (b). Dark current-voltage measurements of Al:ZnO/i-ZnO/CdS/CZTSSe/BC/Mo solar cells: series and shunt resistance (c), and saturation current (J_0) and ideality factor (d).

irrelevant and caused by the fit method. It means that the BC might not affect the diode operation.

Beyond the analysis of PCE of different solar cells, it is remarkable that the median short-circuit current (J_{sc}) is higher for CZTSSe|W (30.2 mA/cm^2) and for CZTSSe|Au (31.5 mA/cm^2) than for CZTSSe|Mo (28.6 mA/cm^2). The latter is in agreement with the results published for CIGS by Jehl Li-Kao *et al.*[17]

To understand these differences, EQE measurements on the best performing CZTSSe solar cells with Mo–, Au–, and W–BC have been carried out and shown on Fig. 6. The quantum efficiency in the visible range is promising (∼90%) for the three cells; the CZTSSe|Mo and

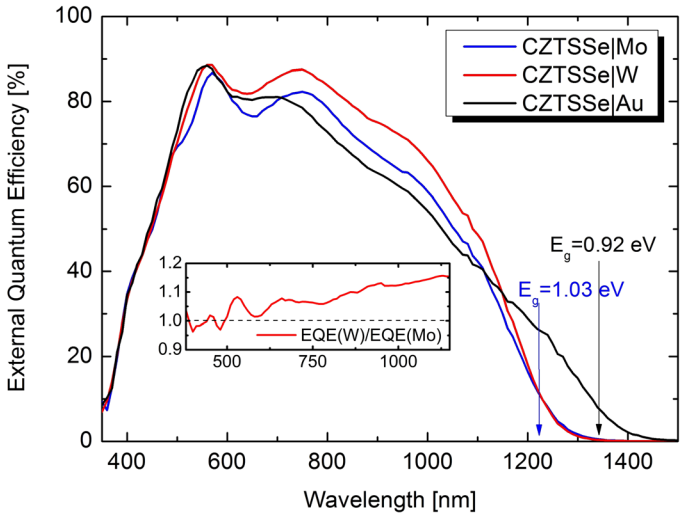

FIG. 6. External quantum efficiency measurements on best performing CZTSSe solar cells with Mo-, Au-, and W-back contacts. Bandgaps E_g are deduced via linear extrapolation of the low energy slope of the EQE. The inset shows EQE spectrum of CZTSSe|W solar cell divided by the EQE spectrum of CZTSSe|Mo solar cell.

CZTSSe|W curves have the same trend in the 380 nm–1300 nm range, although CZTSSe|W shows higher efficiency, whereas CZTSSe|Au EQE is lower between 750 nm and 1150 nm but it is still able to absorb photons in the 1150 nm–1450 nm range. In the inset of Fig. 6, the ratio of quantum efficiencies of cell built on W to cell built on Mo show the wavelength dependence of the current collection. The increase of this ratio at long wavelengths could mean a better collection of carriers generated deep in the absorber in the case of W.

Concerning the gold BC, the more triangular shape of the EQE spectrum is the signature of current collection losses in the absorber. A major difference between CZTSSe|Au and the other cells is the current production in the 1150 nm–1450 nm range. The evaluation of absorber bandgap from EQE curves plotted in Fig. 6 gives 1.03 eV in the case of Mo and W and 0.92 eV in the case of Au. A hypothesis to explain both the decrease of the bandgap and the current collection loss at long wavelengths may be the diffusion of gold partially replacing the copper in the CZTSSe layer close to the back contact. However, this hypothesis has not been clearly confirmed up to now, since no gold diffusion has been evidenced with the different characterization techniques used: GDS is not spatially resolved enough to determine such a diffusion and no shift in XRD spectra has been identified due to potential Au_{Cu} replacement.

IV. CONCLUSIONS

In conclusion, the replacement of Mo back contact in CZTSSe solar cells by other types of metals has been experimentally studied. Results show that, between the different metals used to replace Mo BC, only W and Au are eligible given that they provide a higher current (J_{sc}) compared to Mo. For tungsten this could be explained by a better charge collection in the near infrared part of the solar spectrum. In the case of gold, this effect could be caused by a decrease of the bandgap due to substitution of Cu atoms by Au. In particular, Au has the advantage of not reacting with chalcogens, although CZTSSe synthesized on this BC is irregular at their interface. However, Mo remains the best BC in terms of power conversion efficiency.

ACKNOWLEDGMENTS

The authors thank P. Chapon from Horiba Scientific for the GDS analysis.

[1]C. Persson, J. Appl. Phys. **107**, 53710 (2010).
[2]T. K. Todorov, J. Tang, S. Bag, O. Gunawan, T. Gokmen, Y. Zhu, and D. B. Mitzi, Adv. Energy Mater. **3**, 34–38 (2013).
[3]S. Chen, X. G. Gong, A. Walsh, and S. H. Wei, Appl. Phys. Lett. **94**, 041903 (2009); K. Timmo, M. Altosaar, J. Raudoja, K. Muska, M. Pilvet, M. Kauk, T. Varema, M. Danilson, O. Volobujeva, and E. Mellikov, Sol. Energy Mater. Sol. Cells **94**, 1889 (2010).
[4]C. P. Chan, H. Lam, and C. Surya, Sol. Energy Mater. Sol. Cells **94**, 207 (2010).
[5]M. Patel and A. Ray, Physica B **407**, 4391–4397 (2012).
[6]See http://users.elis.ugent.be/ELISgroups/solar/projects/scaps.html for detailad informations about SCAPS software.
[7]J. J. Scragg, J. T. Wätjen, M. Edoff, T. Ericson, T. Kubart, and C. Platzer-Björkman, J. Am. Chem. Soc. **134**, 19330–19333 (2012).
[8]L. Grenet, S. Bernardi, D. Kohen, C. Lepoittevin, S. Noël, N. Karst, A. Brioude, S. Perraud, and H. Mariette, Sol. Energy Mater. **101**, 11–14 (2012).
[9]P. Jackson, in *Barrieren-Workshop* (Stuttgart, Mars, 2004).
[10]International Center for Diffraction Data: CZTSe—10708930; Cu2SnSe4—10780600; Mo—10714645; PtSe2—107882281.
[11]I. Djerdj, A. M. Tonejc, A. Tonejc, and N. Radić, Vacuum **80**, 1–2 (2005).
[12]P. K. Panigrahi and A. Pathak, Sci. Technol. Adv. Mater. **9**, 045008 (2008).
[13]P. A. Fernandes, P. M. P. Salomé, and A. F. da Cunha, Thin Solid Films **517**, 2519–2523 (2009).
[14]L. Sun, J. He, H. Kong, F. Yue, P. Yang, and J. Chu, Sol. Energy Mater. Sol. Cells **95**, 2907–2913 (2011).
[15]M. Grossberg, J. Krustok, J. Raudoja, K. Timmo, M. Altosaar, and T. Raadik, Thin Solid Films **519**, 7403–7406 (2010).
[16]G. Altamura, L. Grenet, C. Bougerol, E. Robin, D. Kohen, H. Fournier, A. Brioude, S. Perraud, and H. Mariette, "$Cu_2ZnSn(S_{1-x}Se_x)_4$ thin films for photovoltaic applications: Influence of the precursor stacking order on the Selenization process," J. Alloy Compd. (submitted).
[17]Z. Jehl Li-Kao, N. Naghavi, F. Erfurth, J. F. Guillemoles, I. Gérard, A. Etcheberry, J. L. Pelouard, S. Collin, G. Voorwinden, and D. Lincot, Prog. Photovoltaics **20**, 582–587 (2012).